PERGAMON

International Journal of Solids and Structures 39 (2002) 325–340

INTERNATIONAL JOURNAL OF SOLIDS and STRUCTURES

www.elsevier.com/locate/ijsolstr

Nucleation and propagation of an edge crack in a uniformly cooled epoxy/glass bimaterial

E.D. Reedy Jr. *, T.R. Guess

Sandia National Laboratories, P.O. Box 5800, MS-0893, Department 9123, Albuquerque, NM 87185-0893, USA

Received 1 May 2001; in revised form 20 August 2001

Abstract

An epoxy/glass bimaterial beam test configuration has been used to study cooling-induced crack nucleation and propagation. This effort extends a nucleation criterion, previously applied to tensile-loaded, adhesively bonded butt joints, to another geometry and type of loading. Loading by thermally induced straining complicates the application of a nucleation criterion based upon parameters defining the asymptotic stress fields at the interface edge (i.e. at the edge discontinuity defined by the intersection of the interface and stress-free boundary). In contrast to the tensile-loaded butt joint, where the magnitude of asymptotic stress state is fully characterized by a single interface-edge stress intensity factor K_a, an additional, non-negligible r-independent regular term K_{a0} always exists for thermally induced strains. In the present work, a direct extension of the previously used nucleation criterion is applied: crack nucleation occurs when $K_a = K_{ac}$, but with the stipulation that interface-edge toughness K_{ac} depends on K_{a0}. Published by Elsevier Science Ltd.

Keywords: Corner; Cracking; Edge; Epoxy; Fracture; Glass; Interface; Stress singularity; Stress intensity factor

1. Introduction

Bonded and encapsulated bodies frequently contain sharp edges, and failure generally initiates at an interface-edge discontinuity. For example, when an epoxy-bonded butt joint is loaded in tension, cracking will typically originate at the edge discontinuity defined by the intersection of the interface and stress-free boundary (Reedy and Guess, 1993, 1999). One common approach for estimating the strength of such joints is to assume that a preexisting crack emanates from the discontinuity, and then use linear elastic fracture mechanics (LEFM) to determine the load to propagate the crack. The length of the crack used in the LEFM analysis might be based on a detectable limit in a flaw tolerance assessment, or might possibly be based on a representative population of flaws introduced during fabrication.

Even when no crack-like flaws are present, extremely high, though very localized, stresses can exist at an interface edge, a line of geometric and material discontinuity. It is sometimes argued that such stresses have

* Corresponding author. Tel.: +1-505-844-3297; fax: +1-505-844-2762.
E-mail address: edreedy@sandia.gov (E.D. Reedy Jr.).

0020-7683/01/$ - see front matter Published by Elsevier Science Ltd.
PII: S0020-7683(01)00203-7

little effect on the failure process; that the region dominated by the edge discontinuity is too small, that most discontinuities are not truly sharp, or that failure is directly related to the presence of preexisting flaws. Although the stresses associated with an interface edge may have limited impact in many cases, there is compelling evidence that these stresses can indeed induce failure in some joints. For example, a failure criterion, based on the magnitude of interface-edge stresses, accurately predicts how the strength of adhesively bonded butt joints varies with bond thickness and adherend stiffness (Reedy and Guess, 1993, 1997, 1999). In these joints the interface-edge stresses govern crack nucleation, and once nucleated, crack growth is catastrophic.

When viewed asymptotically, an edge discontinuity looks like the apex of a multimaterial wedge. If plane stress or strain applies, then the asymptotic stress state near the apex of dissimilar, isotropic, linear elastic bonded wedges (i.e. at an interface edge (Fig. 1) also referred to as an interface corner in a 2D analysis) has the form

$$\sigma_{ij} = \sum_{n=1}^{N} K_{an} r^{\lambda_n - 1} \bar{\sigma}_{ijn}(\theta) + K_{a0} \bar{\sigma}_{ij0}(\theta) \quad (i, j = r, \theta) \tag{1}$$

where r, θ refer to a polar coordinate system defined at the interface edge. One or more power-law singularities of differing strength can exist, and the exponents can be real or complex (Williams, 1952; Bogy, 1968, 1970, 1971; Hein and Erdogan, 1971). The number of stress singularities N, the strength of these singularities $\lambda_n - 1$, and the angular variation of the stress field associated with each singularity $\bar{\sigma}_{ijn}(\theta)$ are determined by the asymptotic analysis and depend on nondimensional elastic properties (e.g. Dundurs' parameters (Dundurs, 1969)), the local interface-edge geometry (i.e. wedge angle) and edge boundary conditions (stress free, fixed, etc.). The stress intensity factors K_{an} determine the contribution of each singular term to the stress state in the region of the interface edge (Gradin, 1982; Groth, 1988; Hattori et al., 1989; Reedy, 1990; Munz and Yang, 1992; Chen and Nisitani, 1993). The K_{an} depend on global geometry, applied loads and elastic properties. Although not explicitly shown in Eq. (1), there are certain special combinations of elastic properties, wedge angles, and edge loads that can also generate logarithmic singularities (Bogy, 1971; Dempsey, 1995; Chen, 1996).

To date most of our work has utilized an adhesively bonded, tensile-loaded butt joint test geometry that bonds two relatively rigid, sharp-edged, metal cylinders together with a thin, high-strength epoxy adhesive layer. For this geometry and loading, the asymptotic stress state is defined by a single power law singular term, and the strength of the singularity is a real number (Reedy, 1990; Reedy and Guess, 1997). Since a single interface-edge stress intensity factor K_{a1} characterizes the magnitude of the stress state in the region of the interface-edge of a butt joint, it seems reasonable to assume that failure occurs at a critical value of K_{a1}, the interface-edge toughness, K_{ac}. A large body of experimental data shows that a K_{ac} criterion predicts the observed dependence of joint strength on bond thickness (Reedy and Guess, 1993, 1997, 1999). This approach is analogous to LEFM, except that the critical value of the stress intensity factor is associated

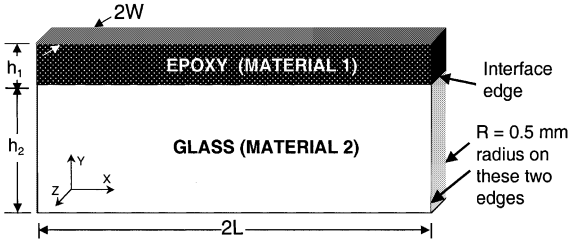

Fig. 1. LOS test geometry.

with a material and geometric discontinuity other than a crack. Here we report work aimed at extending this type of failure analysis to another geometry and type of loading. The test configuration studied casts an epoxy-layer on top of a glass substrate (Fig. 1). In this layer on substrate (LOS) specimen, slow cooling induces edge cracking.

Loading by thermally induced straining complicates the application of a failure criterion based on interface-edge stress fields. The tensile-loaded butt joint and the LOS specimen share the same asymptotic problem: two edge-bonded quarter planes. Consequently, the asymptotic solutions for both types of specimen include a single, power-law singular term. Furthermore, since the strength of the singularity is determined by the asymptotic problem, the strength of the singularity, for a given bimaterial combination and lateral constraint (e.g. plane strain) is the same for both specimens. However, an asymptotic description that includes only the singular term may fail to accurately describe the stress state over a physically significant region about the interface edge when thermal straining occurs. In contrast to the tensile-loaded butt joint, an r-independent regular term $K_{a0}\bar{\sigma}_{ij0}\ (\theta)$ (Eq. (1)) always exists for thermally induced strains (Munz and Yang, 1993; Reedy, 1993). Consequently, it appears unlikely that nucleation is characterized by only a critical K_{a1} value; the effect of K_{a0} must also be considered. Once a crack is nucleated at an edge discontinuity, it might grow stably with increasing load until it reaches a critical length. On the other hand, the load to nucleate cracking might exceed that needed to propagate the nucleated crack. Cracking is then catastrophic; the ultimate failure load is coincident with the load to nucleate cracking. In either case, well-developed fracture mechanics techniques can be used to assess crack growth tendencies.

2. Layer on substrate experiments

A set of 18 LOS samples (Fig. 1, $2L = 123$ mm, $2W = 6.5$ mm), have been tested to determine how epoxy-layer thickness affects the temperature that nucleates cracking in a cooled LOS specimen. The nominal thickness of the epoxy-layer ranged from 1.6 to 6.5 mm (actual thickness was measured after fabrication and ranged from 1 to 6 mm), and the ratio of the epoxy-to-glass thickness, h_1/h_2, was fixed at 0.125. This thickness ratio limits bimaterial beam bending, and the epoxy-layer behaves like a thin film on a thick substrate. A borosilicate float glass was used for the substrate. The substrate's 6.5-mm-wide surfaces were ground with a 20-μm grit wheel, and all edges were left sharp. After cleaning the glass surfaces, the glass substrate was placed at the bottom of a snugly fitted RTV mold, with the cavity depth defining the thickness of the epoxy-layer. The top portion of the mold was filled with a slightly modified version of 3M's EC2216 epoxy adhesive (mix ratio of five parts B to seven parts A, with 2% cabosil added to alter flow characteristics). The epoxy was cured at 65 °C for 14 h followed by 70 °C for 4 h. After cure, the vertical edges on one end of the LOS sample (as indicated in Fig. 1) were ground to a radius of 0.5 mm. This was done to remove 3D interface corners (e.g., a point defined by the intersection two perpendicular edges and a mutually perpendicular interface) since they could possibly influence experimental results (Labossiere and Dunn, 2001). To assure that fracture always initiated on the end of the LOS specimen being watched, a drop of epoxy was placed over the interface edge on the other end. All samples were stored in a desiccated environment prior to testing.

The elastic properties of the glass and epoxy are listed in Table 1. Since the epoxy's glass transition temperature is 15 °C, cooling from the cure temperature induces little residual stress. Although DMA modulus and TMA thermal coefficient of expansion data indicate that E and α_T vary with temperature over the temperature range of interest, (23 to −60 °C), their product, $E\alpha_T$, was found to be essentially independent of temperature over this same temperature range. Note that although the epoxy properties listed in Table 1 were measured at −60 °C, their product is temperature independent. Since cooling induced stress is proportional to the product $E\alpha_T$, an analysis using the properties listed in Table 1 is applicable to the entire temperature range of interest. This was confirmed by performing cooling induced, bimaterial beam bending

Table 1
LOS specimen material properties (v is Poisson's ratio)

	E (GPa)	v	α_T (/°C)
Epoxy[a]	4	0.25	65e − 6
Glass	63	0.20	3e − 6

[a] Properties at −60 °C.

tests. Predicted and measured strains were in good agreement when temperature change was defined with respect to a 10 °C reference temperature.

A liquid-nitrogen-cooled environmental chamber was used to test the LOS specimens. The specimens were cooled at a rate of 1 °C/min. The chamber contained a viewing port, and a video camera with a macrolens recorded the test. There is some limited evidence that very small, isolated, point-like flaws and perhaps small separations developed along the straight interface edge as the temperature decreased. Our images lacked the magnification needed to resolve this level of detail. Even if these edge flaws do exist, they did not grow, nor were they associated in any direct way with the one large crack that eventually formed. In 15 of the 18 tests, the crack that eventually grew and propagated could be clearly associated with a small, isolated flaw that nucleated near the curved portion of the interface edge (i.e., in the vicinity of one of the rounded edges, Fig. 1). This flaw immediately kinked into the glass. With continued cooling, the crack progressed along and across the specimen, eventually following a path that was roughly parallel to the interface. The propagating crack was typically several bond thicknesses long by the time the temperature had decreased an additional 5 °C below that at nucleation. The crack in a LOS specimen with a relatively thick epoxy-layer (>3 mm) tended to run rapidly along the specimen length once the crack front was fully developed. A shard of glass, with a thickness of roughly one-quarter to one-half of that of the epoxy-layer, remained attached to the epoxy-layer. Fig. 2 plots the temperature change $-\Delta T$ at crack nucleation versus epoxy-layer thickness ($-\Delta T$ is plotted since ΔT, the nucleation temperature minus the 10 °C reference

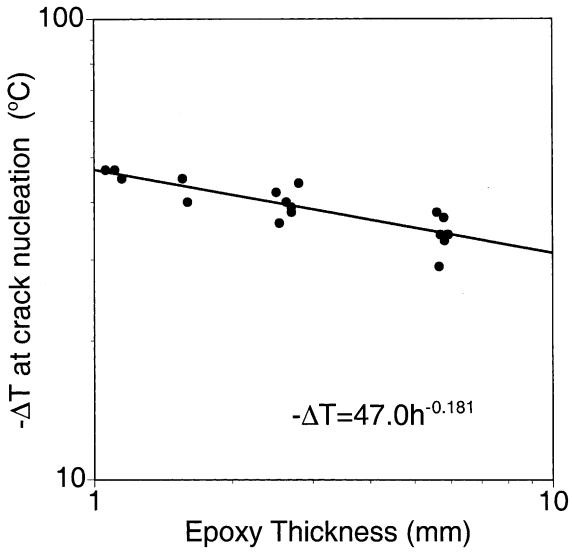

Fig. 2. Change in temperature to nucleate crack growth vs. epoxy-layer thickness (note $-\Delta T$ is plotted, where ΔT equals the nucleation temperature minus the 10 °C reference temperature).

temperature, is a negative number). The magnitude of $-\Delta T$ decreases as the epoxy thickness increases, and on this log–log plot, the decrease is approximately linear with a slope of -0.18.

3. Layer on substrate K_a and K_{a0}

This section presents the K_a and K_{a0} calibrations used to determine the critical K_a and K_{a0} values at crack nucleation from the measured LOS test data. These calibrations relate the value K_a and K_{a0} to temperature change, specimen geometry, and material properties. Relations based on plane stress and plane strain assumptions are presented first, and the importance of including the r-independent K_{a0} in describing interfacial normal stress distributions is assessed. The plane stress and strain calibrations are applicable to the LOS test geometry in only some approximate way, and the applicability of these relations depends on factors such as the epoxy height/width ratio. Furthermore, in the region of the rounded edge, where failure was observed to initiate, the rounded edge itself constrains the deformation. For that reason, full 3D calculations (glass modeled as rigid) were also carried out to better understand the applicability of the plane stress and strain calibrations, and also to suggest corrections to these relationships.

3.1. Calibrations for plane stress and plane strain

Based upon dimensional considerations and linearity with applied load, the stress intensity factor K_a must have the form (dropping the subscript on K_a and λ in Eq. (1) since $N = 1$)

$$K_a = \sigma^* h_1^{1-\lambda} A(\alpha, \beta, h_2/h_1, L/h_1) \tag{2}$$

where σ^* is a characteristic stress, h_1 is a characteristic length, and the function A depends on nondimensional material parameters (i.e. Dundurs' elastic mismatch parameters, α and β) and geometric parameters (e.g. ratio of layer heights h_1/h_2). As noted above, the strength of the stress singularity, $\lambda - 1$, is known from the asymptotic analysis. Consequently, specifying the choices for characteristic stress and length and prescribing the functional dependence of A on all relevant nondimensional geometric and elastic parameters defines the K_a calibration. A convenient choice for the characteristic stress σ^* is the constraint stress developed in a thin compliant layer on a thick, stiff substrate

$$\sigma^* = -E_1[\alpha_{T1} - \alpha_{T2}]\Delta T \quad \text{plane stress} \tag{3}$$

$$\sigma^* = -\frac{E_1}{(1 - \nu_1^2)}[(1 + \nu_1)\alpha_{T1} - (1 + \nu_2)\alpha_{T2}]\Delta T \quad \text{plane strain} \tag{4}$$

where E is Young's modulus and α_T is the coefficient of thermal expansion (subscript 1 for epoxy, 2 for glass) and ΔT is negative for cooling. Likewise a convenient choice for the characteristic length h_1 is the thickness of the epoxy-layer.

The known form of the asymptotic solution was matched with detailed plane stress and plane strain finite element results to determine the value of the function A for epoxy/glass and epoxy/rigid (rigid material has $\alpha_T = 0$) LOS specimens when $h_1/h_2 \ll 1$ and $h_1/L \ll 1$, and using the material properties listed in Table 1. Since $E_1 h_1 \ll E_2 h_2$, bimaterial beam bending is negligible, and the epoxy-layer acts as if it is thin (i.e., there is essentially no through-the-thickness variation in stress in the epoxy-layer when sufficiently far from the stress-free edge). Furthermore, when h_1 is small relative to both h_2 and L, h_1 can be considered to be the only finite length scale and consequently the function A depends only on the elastic mismatch parameters. Table 2 lists the strength $\lambda - 1$ of the asymptotic stress singularity and the value of the function A for epoxy/glass and epoxy/rigid LOS specimens for both plane stress and plane strain. These A values are within a couple of percent of those determined by utilizing a previously published calibration for butt joints

Table 2
Parameters defining plane stress and plane strain singular asymptotic interface-edge solutions for LOS specimen

Materials	α	β	$\lambda - 1$	$A(\alpha, \beta)$
Epoxy/rigid[a]	−1.000	−0.375	−0.219	2.82
Epoxy/rigid[b]	−1.000	−0.333	−0.255	2.06
Epoxy/glass[a]	−0.881	−0.329	−0.165	3.30
Epoxy/glass[b]	−0.878	−0.290	−0.198	2.37

[a] Plane stress.
[b] Plane strain.

in which the more compliant material is thin (Tilscher et al., 1995). The plane strain LOS K_a calibration for the glass/epoxy LOS is

$$K_a = -0.785\ \Delta T h_1^{0.198}\ (\mathrm{MPa\,mm^{0.198}}) \quad \text{plane strain} \tag{5}$$

where ΔT is in °C and h_1 is in mm (substitute Eq. (4) and Table 2 values into Eq. (2)).

The r-independent regular term $K_{a0}\bar{\sigma}_{ij0}(\theta)$ (Eq. (1)) for two bonded quarter planes in plane stress or plane strain simply defines a uniaxial stress parallel to the stress-free edge (i.e. normal to the interface) with magnitude (Tilscher et al., 1995)

$$K_{a0} = \frac{E_1[\alpha_{T1} - \alpha_{T2}]\Delta T}{v_1 - v_2(E_1/E_2)} \quad \text{plane stress} \tag{6}$$

$$K_{a0} = \frac{E_1[(1+v_1)\alpha_{T1} - (1+v_2)\alpha_{T2}]\Delta T}{v_1(1+v_1) - v_2(1+v_2)(E_1/E_2)} \quad \text{plane strain} \tag{7}$$

where $\bar{\sigma}_{\theta\theta 0}(0)$ has been defined to have a value of 1. Note that K_{a0} does not depend on layer thickness, and for an epoxy/glass LOS in plane strain

$$K_{a0} = 1.045\Delta T\ (\mathrm{MPa}) \quad \text{plane strain} \tag{8}$$

where ΔT is in °C. K_a and K_{a0} calibrations for a rigid substrate (material 2) are obtained by setting α_{T2} and E_1/E_2 to zero in Eqs. (3), (4), (6), and (7).

The origin of the r-independent asymptotic term can be understood for the simple case of bonded rigid ($\alpha_T = 0$) and elastic quarter planes subjected to a uniform temperature change. If the epoxy-layer were not attached to the substrate, a temperature change of ΔT would induce expansion relative to the rigid substrate. If plane stress is assumed and $v > 0$, the rigid substrate limit of Eq. (6) defines a uniaxial stress parallel to the stress-free edge (i.e., normal to the interface) of magnitude

$$K_{a0} = \frac{E_1\alpha_{T1}\Delta T}{v_1} \quad \text{plane stress and plane strain} \tag{9}$$

that negates the thermally induced strain that is parallel to the interface and consequently makes the elastic quarter plane compatible with the rigid substrate. This stress is also consistent with the stress-free boundary condition. Consequently, the uniform, interface normal stress state defined by Eq. (9) is the solution of the asymptotic problem.

3.2. LOS interfacial stress distributions

Fig. 3 compares plane strain finite element and interface-edge asymptotic solutions for interfacial stress in a LOS specimen. Note that the asymptotic function $\bar{\sigma}_{ij1}(\theta)$ defining the angular variation in the singular

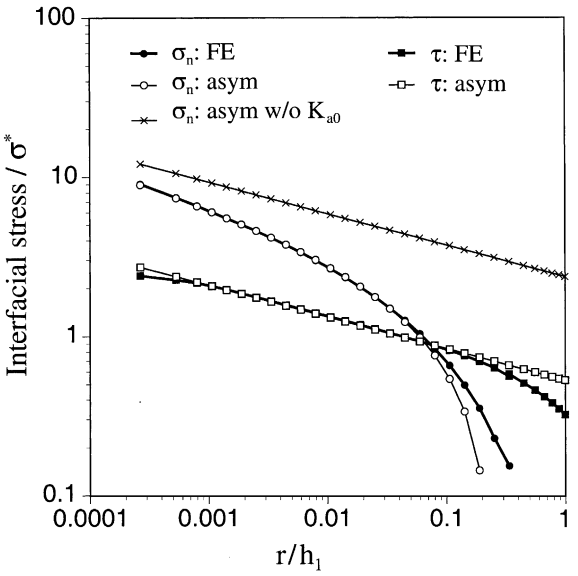

Fig. 3. Plane strain finite element solutions for interfacial normal stress σ_n and interfacial shear stress τ in a uniformly cooled, epoxy/glass LOS specimen are compared with asymptotic (asym) solutions.

stress (Eq. (1)) has been defined to have a value of 1.00 for interfacial normal stress, σ_n, and has a value of 0.225 for interfacial shear stress, τ. The asymptotic solution for interfacial normal stress is simply

$$\sigma_n = K_a r^{\lambda-1} + K_{a0} \tag{10}$$

where K_a and K_{a0} are defined by Eqs. (5) and (8), respectively, and where r is distance from the stress-free edge. Fig. 3 clearly shows that the asymptotic solution σ_n must include the r-independent K_{a0} term to accurately describe the σ_n stress distribution over a physically significant distance. With the inclusion of the K_{a0} term, the asymptotic solution for σ_n and interfacial shear stress, τ, are in very good agreement with finite element results when σ_n and $\tau > \sigma^*$ (i.e., when within the region of elevated stress). The finite element and asymptotic solutions for σ_n and τ are within 5% for $r/h_1 < 0.05$ and $r/h_1 < 0.15$, respectively.

A comparison of plane stress finite element and interface-edge asymptotic solutions is qualitatively similar to the plane strain results shown in Fig. 3. Note, however, that the interfacial tension generated in a yield zone embedded within an elastic, interface-edge stress field is generally higher in plane strain than in plane stress. A plane strain, slip-line theory solution for the asymptotic stress state developed at the interface-edge of a tensile-loaded butt joint with rigid adherends and a rigid-perfectly plastic adhesive layer predicts a hydrostatic interfacial tension of 1.5 σ_y (Reedy and Guess, 1996). Plane strain finite element results for a adhesively bonded, rigid-adherend butt joint verify that an interfacial tension of 1.5 σ_y occurs within the yield zone when an elastic–perfectly plastic adhesive model is used (Reedy and Guess, 1996; Reedy, 2000). In contrast, a plane stress finite element analysis of the same joint shows that the hydrostatic tension within the yield zone is reduced to a level of about 1.0 σ_y.

3.3. 3D geometric effects on LOS asymptotic stress fields

Three-dimensional (3D) finite element calculations were performed to assess how the asymptotic interface-edge stress state in a LOS test specimen differs from that determined by a plane stress or plane strain

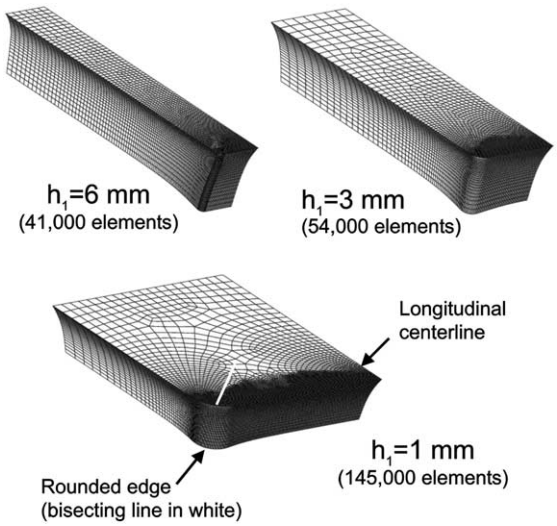

Fig. 4. Finite element meshes used in 3D analysis of a uniformly cooled, epoxy/rigid LOS specimen (deformed mesh shown).

analysis. To make the 3D analysis tractable, the idealized problem of an epoxy-layer on a rigid substrate was analyzed (i.e., the bottom edge of the epoxy-layer was fixed to model the presence of the rigid substrate). Furthermore, by enforcing symmetry conditions, only one-quarter of the LOS specimen had to be modeled, and the length of the LOS specimen was truncated at $L = 4h_1$ (Fig. 1). The plane stress and strain results for the epoxy/glass LOS indicate that at a distance equal to four times the epoxy-layer thickness away from the stress-free edge, the axial stress (i.e., σ_{xx} as defined by the coordinate system shown in Fig. 1) approaches the limit value found in an infinitely long LOS (the calculated σ_{xx} is within 5% of the expected limit value). Accordingly, the interface-edge stress state calculated using a model with $L = 4h_1$ should reasonably approximate the long adherend limit. Three models, with differing epoxy-layer height, were analyzed ($h_1 = 1$, 3, or 6 mm, $2L = 8$, 24, and 48 mm, and $2W = 6.5$ mm; see Fig. 4). As shown in Fig. 4, each of the three models incorporates the 0.5 mm radius R found on the vertical edges of the tested LOS specimens (Fig. 1). Eight-node linear brick elements were use in the analysis, and the meshes were sufficiently refined in the region of the interface-edge to resolve the singular stress fields (characteristic element length-to-layer thickness ratio of 0.017 at the interface-edge).

Fig. 5 compares 3D finite element results for interfacial normal stress along the LOS specimen's longitudinal centerline with asymptotic plane stress and plane strain solutions (parameters used in the epoxy/rigid asymptotic solutions are listed in Table 2). Note that in Fig. 5, distance r is measured from the stress-free edge and finite element results are plotted for three different epoxy-layer thicknesses. A comparison of the plane stress and plane strain asymptotic solutions shows that, at any given r/h_1, the stress level is higher for plane strain, suggesting that this is the harsher condition. The calculated σ_n stress distributions for specimens with $h_1 = 6$ and 3 mm ($W/h_1 = 0.54$ and 1.08, respectively) are nearly identical to the plane stress asymptotic stress distribution (Fig. 5). On the other hand when $h_1 = 1$ mm ($W/h_1 = 3.25$), the calculated stress distribution is instead most like the plane strain asymptotic stress distribution. As the epoxy's width-to-height ratio increases, the solution transitions from a plane stress-like condition to a plane strain-like condition. Recall that at a distance equal to four times the epoxy-layer thickness away from the stress-free edge, the stress state approaches the limit value found in an infinitely long LOS. Consequently, when $W/h_1 = 3.25$, and since the substrate is rigid and $L/h_1 = 4.00$, a condition approximating plane strain is expected.

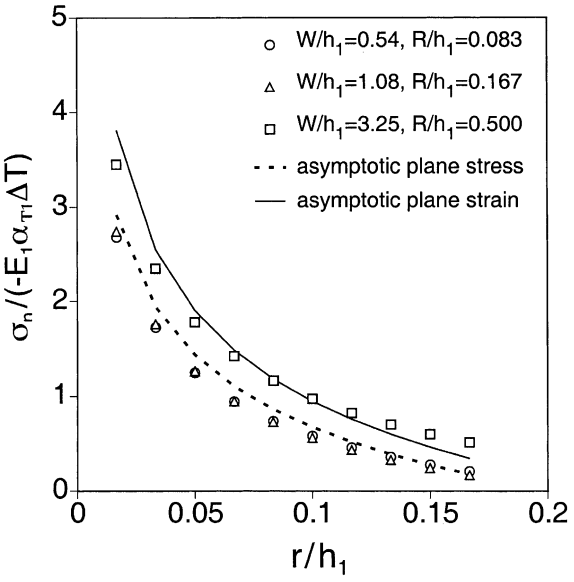

Fig. 5. Comparison of 3D finite element solutions for σ_n along the LOS specimen's longitudinal center line with asymptotic plane stress and plane strain solutions.

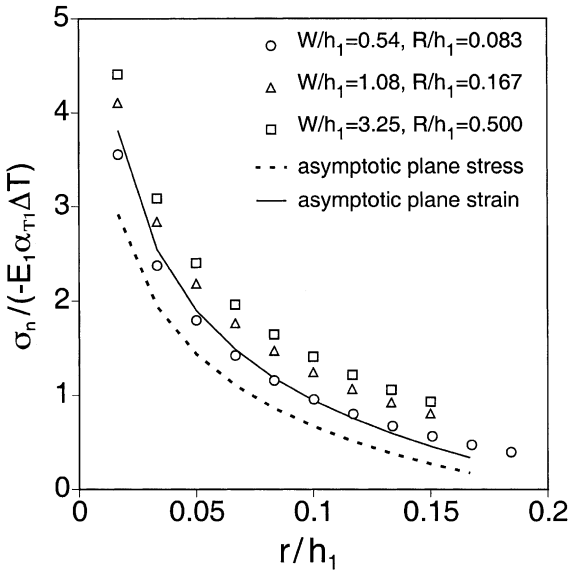

Fig. 6. Comparison of 3D finite element solutions for σ_n along the line bisecting the LOS specimen's rounded edge with asymptotic plane stress and plane strain solutions.

Fig. 6 plots interfacial normal stress along the line bisecting the LOS's rounded edge (along a radius of the circle defining the rounded edge, at an angle of 45° from the longitudinal axis (Fig. 4)). The calculated σ_n stress distributions for $h_1 = 6$ ($W/h_1 = 0.54$) is nearly identical to the plane strain asymptotic stress

distribution, while those for $h_1 = 3$ and 1 mm ($W/h_1 = 1.08$ and 3.25, respectively) lie above the plane strain result. The existence of plane strain-like conditions in the region of a rounded edge seems reasonable since the rounded edge itself constrains deformation. For example, consider a thin epoxy-layer on a rigid, circular substrate. Asymptotic interface-edge stress fields for this axisymmetric geometry will approach the plane strain limit as the epoxy layer-to-disk radius ratio decreases.

Since calculated asymptotic stress distributions at the rounded LOS edge are so similar to the plane strain asymptotic result, the 3D rounded edge stress distributions are expected to have the same asymptotic form (Eq. (10)). The r-independent term K_{a0}, as defined in Eq. (9) for plane stress and plane strain, should apply to the 3D LOS. As discussed in Section 3, K_{a0} simply corresponds to a uniaxial stress parallel to the stress-free edge that negates the thermally induced strain, and indeed K_{a0} has the same value in plane stress and plane strain. If the asymptotic stress distribution at the rounded edge has the same form as the plane strain asymptotic stress distribution, then in the region dominated by the asymptotic field, a plot of $\log(\sigma_n - K_{a0})$ vs. $\log(r)$ will be a straight line with a slope equal to the strength of the plane strain stress singularity (Eq. (10) and Table 2). Log–log plots of the 3D calculated results shown in Fig. 6 do display the expected linear dependence as the interface-edge is approached. Furthermore, the values of the calculated initial slopes (-0.248, -0.245, and -0.245 for $h_1 = 1$, 3, and 6 mm, respectively) are in good agreement with the theoretical, plane strain asymptotic result (-0.255). It is also possible to determine the value of K_a from the log–log plots and these values can then be used to define K_a calibrations for stress along the line bisecting the LOS's rounded edge. Guided by the general form of K_a (Eq. (2)), the rounded corner K_a will be defined in the same way as the plane strain K_a (i.e., σ^* is the rigid substrate limit of Eq. (4)), but the function A will be modified to include the effect of the rounded edge and h_1/W. Table 3 shows that the value of the function A, defined for stress along the line bisecting the rounded edge, varies in a nearly linear manner with h_1/W (i.e., rounded edge A/plane strain $A = 1.1040 - 0.072h_1/W$).

Results for the epoxy/rigid LOS suggests that the function A, used in the K_a calibration for interfacial stress on line bisecting rounded edge LOS, can be defined as a multiplicative correction factor to the plane strain A. This correction factor depends linearly on h_1/W (for a fixed R/W, here $R/W = 0.154$). Since epoxy/glass can be approximated as epoxy/rigid (glass and epoxy Young's modulus differ by a factor of 15, Table 1), it seems reasonable to apply the epoxy/rigid correction to the epoxy/glass plane strain A to produce an approximate calibration for K_a applicable to the rounded edge of an epoxy/glass LOS. Therefore, after modifying Eq. (5)

$$K_a = -0.785\left(1.104 - 0.072\frac{h_1}{W}\right)\Delta T h_1^{0.198}\ (\mathrm{MPa\,mm^{0.198}}) \quad \text{rounded edge} \tag{11}$$

for $L/W \geqslant 4$, $R/W = 0.154$ and where ΔT is in °C and h_1 is in mm. Note that K_{a0} at the rounded edge has the same value as it does in plane strain (Eq. (8)).

Table 3
Parameters defining singular asymptotic interface-edge solutions for stress along a line that bisects the rounded edge of an epoxy/rigid LOS specimen (3D model)

h_1 (mm)	L/h_1	W/h_1	R/h_1	$\lambda - 1$	Rounded edge A	Rounded edge A/Plane strain A
1	4.00	3.25	0.500	−0.255	2.22	1.08
3	4.00	1.08	0.167	−0.255	2.14	1.04
6	4.00	0.54	0.083	−0.255	2.00	0.97

4. K_a vs. K_{a0} crack nucleation criterion

The parameters defining the asymptotic, interface-edge stress field are a potential basis for a crack nucleation criterion provided that (1) cracking actually nucleates at the interface edge, (2) the edge appears sharp on a length scale commensurate with that of the asymptotic stress field, and (3) the nucleation zone, as well as any surrounding yield-like zone, is deeply embedded within the region dominated by the asymptotic stress state. When these conditions are met, K_a and K_{a0} uniquely define of the intensity of the stress field at the edge, independent of global geometry and details of the applied loading. These restrictions are analogous to the familiar small-scale yielding requirement of linear elastic fracture mechanics.

The LOS test data can be used to assess the applicability of a crack nucleation criterion based upon measured K_a and K_{a0} values at nucleation. Fig. 2 shows that the ΔT at crack nucleation varies with layer thickness, h_1. Each ΔT, h_1 pair defines a critical K_a value and an associated K_{a0}. In the present work, a rather simple nucleation criterion is considered: it is assumed that crack nucleation occurs when $K_a = K_{ac}$, with the stipulation that interface-edge toughness K_{ac} depends on K_{a0}. Since cracking in an epoxy/glass LOS specimen nucleates at the rounded interface edge, the rounded edge K_a calibration (Eq. (11)) is used in conjunction with the Fig. 2 data to determine K_{ac} values while Eq. (8) is used to determine the associated value of K_{a0}. Fig. 7 clearly suggests that there is a moderate increase in K_{ac} as K_{a0} becomes increasingly compressive ($-K_{a0}$ is plotted since K_{a0} is compressive for cooling). This is the expected trend since a higher K_{ac} would be needed to compensate for the addition of an increasingly compressive K_{a0}. Although the scatter in the data makes it difficult to define the dependence of K_{ac} on K_{a0}, a least squares fit of the plotted data indicates that

$$K_{ac} = 21.5 - 0.42K_{a0} \quad (\mathrm{MPa\,mm^{0.198}}) \tag{12}$$

where K_{a0} is in MPa.

For a particular epoxy/glass LOS specimen geometry (i.e., for a given h_1 and h_1/W), the temperature at crack nucleation can be predicted by setting Eq. (11) equal to Eq. (12) (i.e., $K_a = K_{ac}$), substituting Eq. (8)

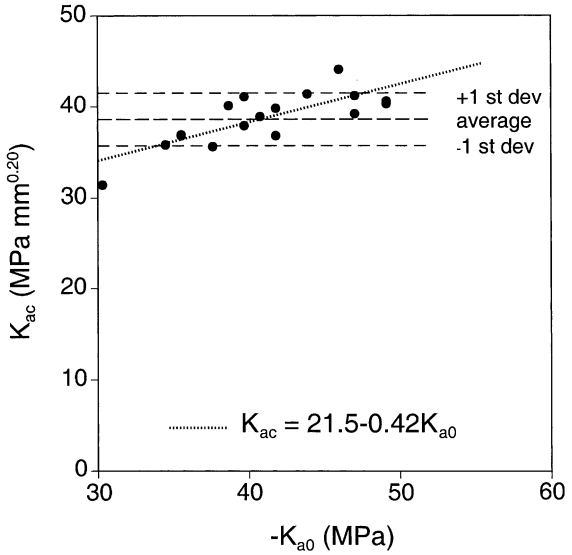

Fig. 7. K_{ac} vs. the associated K_{a0} (using the rounded interface-edge K_a calibration).

Table 4
Temperature change to nucleate cracking consistent with $K_a = K_{ac} = 21.5 - 0.42K_{a0}$ nucleation criterion for a range of epoxy-layer thickness

h_1 (mm)	ΔT (°C)	K_{a0} (MPa)	K_{ac} (MPa mm$^{0.20}$)
1	−52.4	−54.8	44.5
3	−37.5	−39.2	38.0
6	−33.2	−34.7	36.1

for K_{a0}, and then solving for ΔT. For example, Table 4 uses Eq. (12) to predict ΔT at crack nucleation for $h_1 = 1$, 3, and 6 mm. Table 4 also lists the associated K_{ac} and K_{a0} values, and the asymptotic σ_n distributions corresponding to these parameters (i.e., substituting these values into Eq. (10)) are plotted in Fig. 8. The experimentally determined K_{ac} relationship (Eq. (12)) gives rise to nearly identical σ_n distributions for $h_1 = 1$, 3, and 6 mm. Since the crack nucleation process is almost certainly dependent on σ_n at the interface edge, this consistency in σ_n distributions lends support to a nucleation criterion that uses a K_{a0}-dependent, interface-edge toughness.

As an aside, the use of the rounded, interface-edge K_a calibration, as determined by 3D finite element analysis, is a necessary element in the determination of the crack nucleation criterion. If the 2D plane strain K_a calibration (Eq. (5)) is used instead, the resulting K_{ac} vs. K_{a0} data show no definitive trend (Fig. 9). These interface toughness values are reasonably consistent (average $K_{ac} = 37.6$ MPa mm$^{0.20}$, with a standard deviation/average of 0.07). Consequently, it might seem reasonable to conclude that $K_a = K_{ac}$ (where K_a is the plane strain calibration and K_{ac} is a K_{a0}-independent constant) is a valid crack nucleation criterion. However, a nucleation criterion based upon the plane strain K_a calibration and $K_{ac} = 37.6$ MPa mm$^{0.20}$ give rise to σ_n distributions for $h_1 = 1$, 3, and 6 mm that lack consistency (Fig. 10; for each h_1, Eq. (5) is solved for ΔT, K_{a0} is determined from Eq. (8), and σ_n is determined using Eq. (10)).

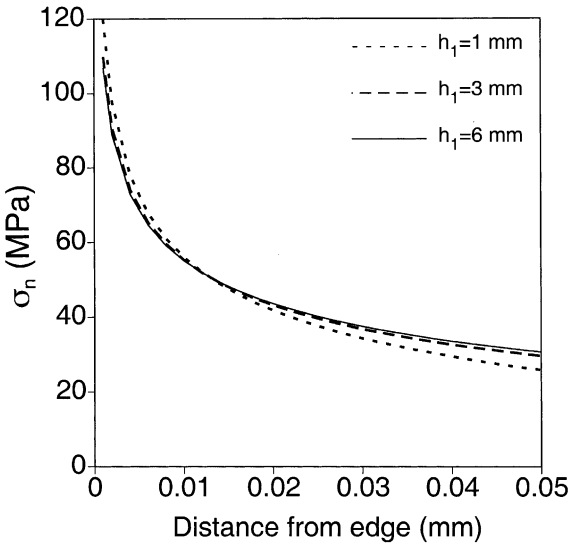

Fig. 8. Asymptotic σ_n when $K_a = K_{ac}$ nucleation criterion is satisfied (using rounded interface-edge K_a calibration and $K_{ac} = 21.5–0.42K_{a0}$ MPa mm$^{0.20}$).

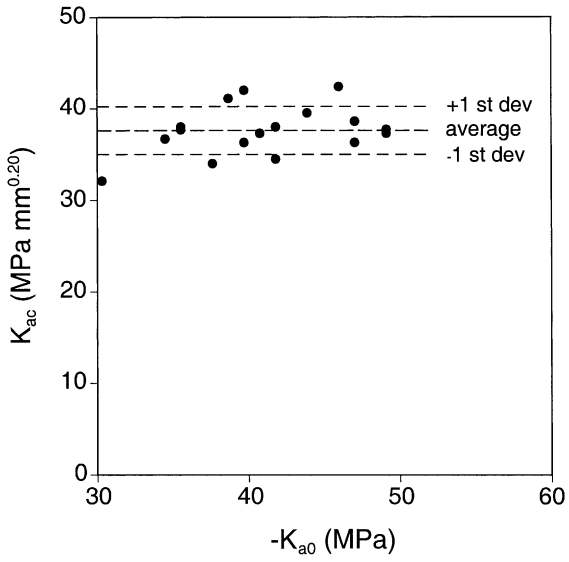

Fig. 9. K_{ac} vs. the associated K_{a0} (using the plane strain K_a calibration).

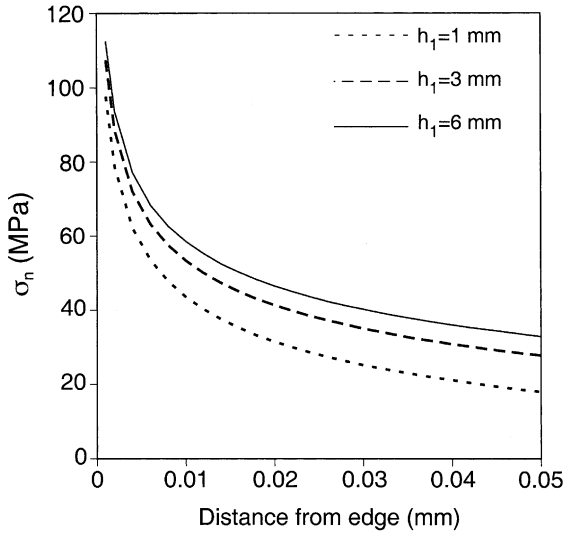

Fig. 10. Asymptotic σ_n when $K_a = K_{ac}$ nucleation criterion is satisfied (using the plane strain K_a calibration and $K_{ac} = 37.6$ MPa mm$^{0.20}$).

5. Crack propagation

There is a well-developed understanding of steady-state substrate cracking in pre-tensioned thin film/brittle substrate bimaterials (Thouless et al., 1987; Drory et al., 1988; Hu et al., 1988; Suo and Hutchinson, 1989; Chiao and Clarke, 1990). The key observation is that the crack follows a trajectory parallel to the interface with a depth governed by a $K_{II} = 0$ criterion (Thouless et al., 1987). The steady-state cracking depth

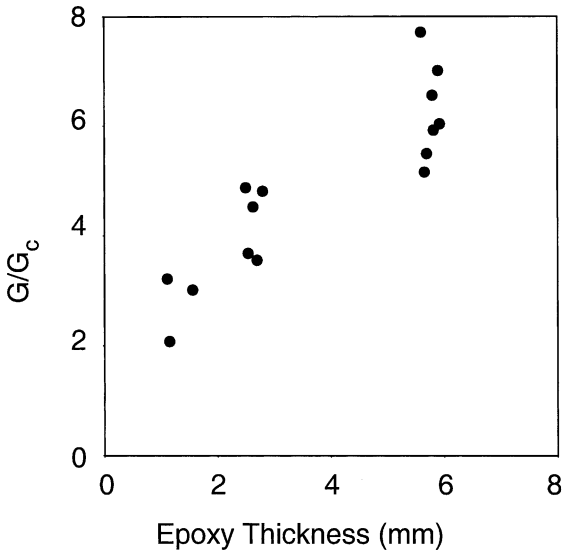

Fig. 11. G/G_c at the ΔT when the nucleated crack was observed to be at least several bond thicknesses long vs. epoxy-layer thickness.

and the associated energy release rate in an infinitely long bimaterial can be determined as a function of film/substrate thickness, elastic properties, and temperature change using formulas published by Suo and Hutchinson (1989). Recall that LOS specimens have a nominal epoxy-to-glass thickness ratio of 0.125 and an epoxy thickness that ranges from 1 to 6 mm. For these geometric parameters and the elastic properties listed in Table 1, $G/G_I \sim 0.8$, where G is the plane stress energy release rate at the steady-state cracking depth and G_I is the plane stress energy release rate for a semi-infinite interfacial crack between a thin film and a thick substrate ($G_I = \sigma^{*2} h_1/2E_1$ where the plane stress constraint stress σ^* is defined in Eq. (3)). Fig. 11 plots the energy release rate corresponding to the calculated steady-state crack depth at the ΔT that the nucleated crack was observed to be at least several bond thicknesses long (typically at a ΔT 5 °C below that at nucleation) vs. epoxy layer thickness. Note that G is normalized by the borosilicate glass's G_c, where $G_c = 8$ J/m^2 (Mecholsky et al., 1974). The magnitude of the ΔT required to nucleate cracking in the LOS tests exceeds that required for steady-state substrate cracking. Furthermore, G/G_c ratio increases rapidly with epoxy-layer thickness. This result is consistent with experimental observation; the crack in a LOS specimen with a relatively thick epoxy-layer (>3 mm) ran rapidly along the specimen length once the crack front was fully developed.

6. Conclusions

A crack nucleation criterion that had been previously applied to tensile-loaded, adhesively bonded butt joints has been extended and applied to another geometry and type of loading. The test configuration casts an epoxy-layer on top of a glass substrate, and the specimen is loaded by slow cooling. Although the following observations apply specifically to the epoxy/glass bimaterial LOS specimens tested in the present study, these results may also apply to other bimaterial combinations that generate tensile, interface-edge normal stress via cooling of a relatively thin, compliant layer on a stiff, brittle substrate.

- Slow cooling nucleates cracking along the portion of the interface edge where a 0.5 mm radius provides a transition between the lateral and longitudinal LOS interface edges.

- The temperature change that nucleates cracking depends on the epoxy-layer thickness: the temperature change for nucleation increased by 40% as the epoxy-layer thickness was decreased from 6 to 1 mm.
- The asymptotic solution for interfacial normal stress σ_n must include the r-independent K_{a0} term to accurately describe the σ_n stress distribution over a physically significant distance.
- A K_a calibration applicable to the rounded edge of an epoxy/glass LOS can be defined as a correction factor applied to the plane strain calibration.
- Crack nucleation occurs when $K_a = K_{ac}$, where interface-edge toughness K_{ac} depends on K_{a0}.
- The experimentally determined K_{ac} vs. K_{a0} relation gives rise to nearly identical σ_n distributions in LOS specimens with 1-, 3-, and 6-mm thick epoxy-layers.
- The magnitude of the ΔT required to nucleate cracking in the LOS tests exceeds that required for steady-state substrate cracking.

Acknowledgements

This work was performed at Sandia National Laboratories. Sandia is a multiprogram laboratory operated by Sandia corporation, a Lockheed Martin company, for the US department of energy under contract DE-AC04-94AL85000.

References

Bogy, D.B., 1968. Edge-bonded dissimilar orthogonal elastic wedges under normal and shear loading. Journal of Applied Mechanics 35, 460–466.

Bogy, D.B., 1970. On the problem of edge-bonded elastic quarter-planes loaded at the boundary. International Journal of Solids and Structures 6, 1287–1313.

Bogy, D.B., 1971. Two edge-bonded elastic wedges of different materials and wedge angles under surface tractions. Journal of Applied Mechanics 38, 377–386.

Chen, D.-H., 1996. Logarithmic singular stress field in a semi-infinite plate consisting of two edge-bonded wedges subjected to surface tractions. International Journal of Fracture 75, 357–378.

Chen, D.-H., Nisitani, H., 1993. Singular stress field near the corner of jointed dissimilar materials. Journal of Applied Mechanics 60, 607–613.

Chiao, Y.-H., Clarke, D.R., 1990. Residual stress induced fracture in glass-sapphire composites: planar geometry. Acta Metallurgica et Materialia 38, 251–258.

Dempsey, J.P., 1995. Power-logarithmic stress singularities at bi-material corners and interface cracks. Journal of Adhesion Science and Technology 9, 253–265.

Drory, M.D., Thouless, M.D., et al., 1988. On the decohesion of residually stressed thin films. Acta Metallurgica 36, 2019–2028.

Dundurs, J., 1969. Discussion of edge-bonded dissimilar orthogonal elastic wedges under normal and shear loading. Journal of Applied Mechanics 36, 650–652.

Gradin, P.A., 1982. A fracture criterion for edge-bonded bimaterial bodies. Journal of Composite Materials 16, 448–456.

Groth, H.L., 1988. Stress singularities and fracture at interface corners in bonded joints. International Journal of Adhesion and Adhesives 8, 107–113.

Hattori, T., Sakata, S., et al., 1989. A stress singularity parameter approach for evaluating the interfacial reliability of plastic encapsulated LSI devices. Journal of Electronic Packaging 111, 243–248.

Hein, V.L., Erdogan, F., 1971. Stress singularities in a two-material wedge. International Journal of Fracture 7, 317–330.

Hu, M.S., Thouless, M.D., et al., 1988. The Decohesion of Thin Films from Brittle Substrates. Acta Metallurgica 36, 1301–1307.

Labossiere, P.E.W., Dunn, M.L., 2001. Fracture initiation at three-dimensional bimaterial interface corners. Journal of the Mechanics and Physics of Solids 49, 609–634.

Mecholsky, J.J., Rice, R.W., et al., 1974. Prediction of Fracture Energy and Flaw Size in Glasses from Measurements of Mirror Size. Journal of The American Ceramic Society 57, 440–443.

Munz, D., Yang, Y.Y., 1992. Stress Singularities at the interface in bonded dissimilar materials under mechanical and thermal loading. Journal of Applied Mechanics 59, 857–861.

Munz, D., Yang, Y.Y., 1993. Stresses near the edge of bonded dissimilar materials described by two stress intensity factors. International Journal of Fracture 60, 169–177.

Reedy Jr., E.D., 1990. Intensity of the stress singularity at the interface corner between a bonded elastic and rigid layer. Engineering Fracture Mechanics 36, 575–583.

Reedy Jr., E.D., 1993. Asymptotic interface corner solutions for butt tensile joints. International Journal of Solids and Structures 30, 767–777.

Reedy Jr., E.D., 2000. Connection between interface corner and interfacial fracture analyses of an adhesively bonded butt joint. International Journal of Solids and Structures 37, 2429–2442.

Reedy Jr., E.D., Guess, T.R., 1993. Comparison of butt tensile strength data with interface corner stress intensity factor prediction. International Journal of Solids and Structures 30, 2929–2936.

Reedy Jr., E.D., Guess, T.R., 1996. Interface corner stress states: plasticity effects. International Journal of Fracture 81, 269–282.

Reedy Jr., E.D., Guess, T.R., 1997. Interface corner failure analysis of joint strength: effect of adherend stiffness. International Journal of Fracture 88, 305–314.

Reedy Jr., E.D., Guess, T.R., 1999. Additional interface corner toughness data for an adhesively-bonded butt joint. International Journal of Fracture 98, L3–L8.

Suo, Z., Hutchinson, J.W., 1989. Steady-state cracking in brittle substrates beneath adherent films. International Journal of Solids and Structures 25, 1337–1353.

Thouless, M.D., Evans, A.G., et al., 1987. The edge cracking and spalling of brittle plates. Acta Metallurgica 35, 1333–1341.

Tilscher, M., Munz, D., et al., 1995. The stress intensity factor in bonded quarter planes after a change in temperature. Journal of Adhesion 49, 1–21.

Williams, M.L., 1952. Stress singularities resulting from various boundary conditions in angular corners of plates in extension. Journal of Applied Mechanics 19, 526–528.